Snow Parameter Estimation Using Multiple Squint Differential InSAR: A Potential Application for the Harmony Mission

Andreas Benedikter, Kristina Belinska, Marc Rodriguez-Cassola, Pau Prats-Iraola, and Gerhard Krieger
Microwaves and Radar Institute, German Aerospace Center (DLR), Germany, andreas.benedikter@dlr.de

Abstract

Spaceborne differential SAR interferometry for snow water equivalent (SWE) change measurements is known to be limited by: i) low coherence areas resulting from temporal decorrelation, largely complicating a robust phase unwrapping, ii) inaccurate density estimates introducing systematic errors in the phase-to-SWE inversion, and iii) an unknown phase offset due to the 2π ambiguity of the interferometric measurement and therefore a strongly biased SWE estimate. This paper presents strategies to overcome these shortcomings by exploiting simultaneously acquired interferograms with different squint angles. The phase difference between the interferograms may be exploited to resolve the 2π phase ambiguity of the single interferogram. In addition to that, the ratio between the interferograms is a measure of the dielectric permittivity of the snow and can be related to the snow density. The performance of the strategies is evaluated for ESA's Harmony mission, demonstrating great potential of the approach given the large squint diversity of the Harmony constellation.

1 Introduction

Snow water equivalent (SWE) is an important indicator used in hydrology, glacier mass balance, and climate change impact. SWE is defined as the depth of water which would result if all the ice contained in the snow pack were melted. The potential of differential SAR interferometry (D-InSAR) to measure SWE change has been demonstrated in several studies [1, 2, 3, 4]. Despite being demonstrated over 20 years ago by Guneriussen et al. [1], D-InSAR SWE mointoring is not applied operationally, mainly because of the following limiting factors:

- low temporal coherence areas limit the accuracy of the phase measurement and may significantly complicate the phase-unwrapping process down to a point at which no robust SWE retrieval is possible,
- the phase-to-SWE inversion requires an estimate of the snow density, which is commonly not accurately known, resulting in systematic errors,
- a reference point with known SWE change is required in the scene to estimate the absolute phase because the D-InSAR phase may carry an unknown offset if the phase delay introduced by the propagation through snow surpasses 2π.

In this paper, we show that the absolute phase can be robustly estimated by exploiting the phase difference between two or more interferograms with different squint angles that are acquired simultaneously. A comparable approach has been suggested in [5] for measuring the absolute troposphere change. Furthermore, the ratio of two interferograms with different squint angles is a direct measure of the real part of the dielectric permittivity of the snow and can be linked to the snow density, which is an important input for the D-InSAR SWE mapping but also for other sensor concepts and modeling approaches.

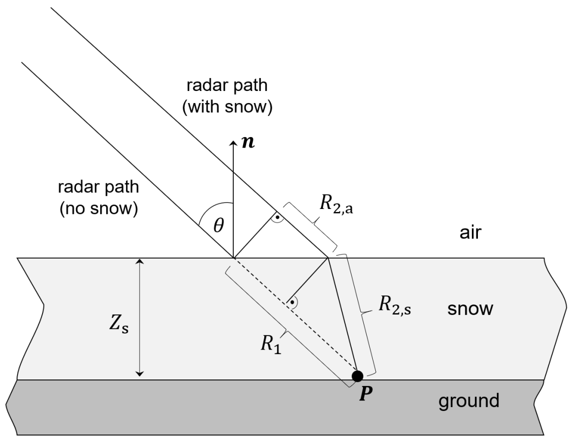

Figure 1 Geometry of the refraction effect in snow.

The planned Earth Explorer 10 mission, Harmony [6], turns out to be a perfect candidate for the proposed approach due to the large squint diversity of the constellation and is therefore chosen as an example case to evaluate the potential performance of the approach. Also, the Co-Fliers concepts from NASA JPL [7] would be perfect candidates to implement the proposed techniques.

2 D-InSAR SWE Measurement

Sufficiently dry snow is almost transparent at microwave frequencies. Therefore, the backscatter contribution from the snow surface and volume can be expected to be much less than the backscatter from the underlying ground. The

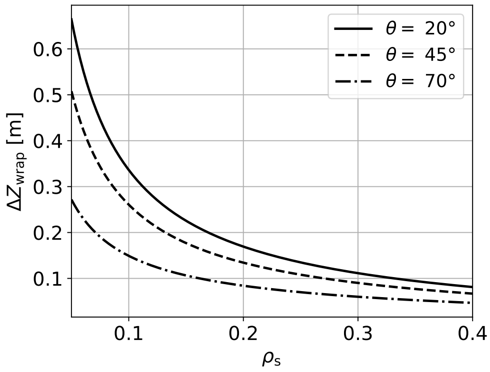

Figure 2 Critical limit of snow height change at which the first phase wrap in the D-InSAR interferogram occurs. Shown for the Harmony/Sentinel-1 5.405 GHz center frequency, different snow densities and incident angles.

higher relative dielectric permittivity of snow ε_{s} compared to air results in a reduced propagation velocity of the radar signals within the snowpack and therefore refraction at the air-snow interface, as shown in **Figure 1**. If we assume a constant snow density profile through the snow pack, the SWE change, ΔSWE, is related to the snow height change, ΔZ_{s}, by

$$\Delta\mathrm{SWE} = \Delta Z_{\mathrm{s}} \cdot \rho_{\mathrm{s}}, \tag{1}$$

and, according to [1], the D-InSAR phase resulting from a SWE change can be written as:

$$\Delta\Phi_{\mathrm{s}} = \Delta\mathrm{SWE} \cdot \frac{4\cdot\pi}{\lambda\cdot\rho_{\mathrm{s}}} \cdot \left(\sqrt{\varepsilon_{\mathrm{s}}(\rho_{\mathrm{s}}) - \sin^2\theta} - \cos\theta\right), \tag{2}$$

where λ is the wavelength, ρ_{s} is the snow density (normalized by the density of water) , $\varepsilon_{\mathrm{s}}(\rho_{\mathrm{s}})$ is the density dependent relative permittivity of the snowpack, and θ is the incident angle. We assume here a constant snow density (i.e., a mean density), an approximation that is well suited also for stratified snowpacks [3]. Following [3], the relative permittivity of the snowpack can be computed as

$$\varepsilon_{\mathrm{s}}(\rho_{\mathrm{s,abs.}}) = 1 + 1.5995 \cdot \rho_{\mathrm{s,abs.}} + 1.861 \cdot \rho^3_{\mathrm{s,abs.}}, \tag{3}$$

where $\rho_{\mathrm{s,abs.}}$ is the absolute snow density in $\mathrm{g\,cm^{-3}}$.

An unknown offset in the D-InSAR ΔSWE measurement results, if the snow height change leads to a D-InSAR phase greater than 2π. **Figure 2** shows the critical snow height change that leads to phase wrapping (ΔZ_{wrap}) for different relative snow densities ranging from calmly fallen to heavily wind-compacted dry snow and three incident angles. Note that only dry snow conditions are considered. Beyond ΔZ_{wrap}, the conventional D-InSAR ΔSWE retrieval does not produce meaningful results if no reference point with known ΔSWE value is present in the scene. The plots are shown for the Harmony and Sentinel-1 mission center frequency of 5.405 GHz (C band). For most of the snow states, already a snow height change of 20 cm leads to phase wrapping. This allows the conclusion that at C band or higher frequencies conventional D-InSAR ΔSWE mapping cannot be used for a large variety of snowfall events.

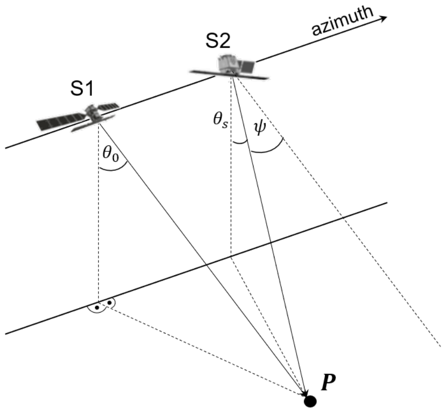

Figure 3 Illustration of the squinted acquisition geometry (S2) compared to a zero-squint acquisition (S1).

3 Exploiting Multiple Squints

The phase contribution due to the signal propagation through snow depends on the local incident angle, which, is a function of the squint angle. Hence, for a squinted acquisition, the net phase corresponds to an incident angle that is larger than the boresight incident angle. **Figure 3** illustrates the concept for a zero-squint acquisition (S1) and an acquisition with a squint angle $|\psi| > 0$ (S2). Assuming a flat Earth geometry and a linear radar track, the difference between the D-InSAR phase of a squinted acquisition and a zero-squint acquisition is shown in **Figure 4**. The 5.405 GHz frequency is used and a ΔSWE of 3.5 cm is assumed. The solid (black) contours correspond to a relative snow density of 0.1 and the dashed (red) contours to 0.4. The phase difference increases for larger squint angle differences and hence, also the sensitivity of the differential D-InSAR phase to the ΔSWE increases. Due to the small snow height compared to the satellite altitude, it can be assumed that even for large squint angle differences, the ΔSWE seen by two simultaneous D-InSAR acquisitions will be largely correlated.

In the following subsections, three approaches for exploiting simultaneously acquired interferograms with different squint angles are analyzed for low to moderate coherence scenarios. The analyses are based on a setting with two sensors (S1 and S2) both acquiring data simultaneously, one with zero squint and the other with a squint greater than zero, as shown in Figure 3. Both sensors acquire repeat-pass interferograms. We assume monostatic acquisitions in the following derivations but draw conclusions to the bistatic nature of the Harmony mission.

The Harmony mission consists of two companion satellites to Sentinel-1 as bistatic receivers (cf. **Figure 5**). The two Harmony satellites are flying 350 km in front and behind Sentinel-1 in two different configurations. In both configurations, there is a squint diversity between the Harmony satellites and Sentinel-1 of roughly 22° (i.e., ≈11° effective squint due to the bistatic operation of the Harmony satellites).

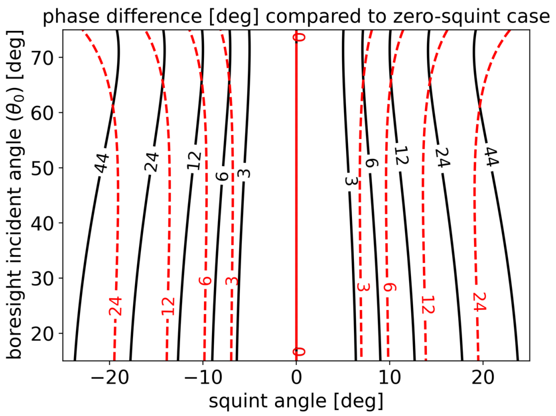

Figure 4 Snow induced phase difference of a squinted D-InSAR acquisition (S2) compared to the zero-squint case (S1). Values are shown for the 5.405 GHz center frequency, a ΔSWE of 3.5 cm, and two density values: $\rho_s = 0.1$ (solid, black) and $\rho_s = 0.4$ (dashed, red).

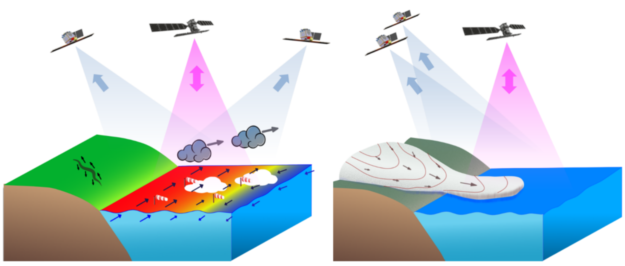

Figure 5 Illustration taken from [8] showing the Harmony constellation in the (left) StereoSAR configuration and (right) XTI formation.

3.1 Low-Resolution Absolute ΔSWE Estimation

ΔSWE mapping using D-InSAR commonly requires phase unwrapping to recover the spatial variation of the SWE and a reference point in the scene with known ΔSWE to recover the bulk phase offset over the scene. However, in low-coherence scenarios it may be infeasible to perform robust phase unwrapping. In such cases the difference phase, $\Delta\Delta\Phi_s$, between the two interferograms may be exploited since it has a significantly reduced sensitivity to the ΔSWE compared to the single interferograms. Therefore, $\Delta\Delta\Phi_s$ stays within a single 2π interval for a large range of ΔSWE values. The D-InSAR phases of the two acquisitions can be written as

$$\begin{aligned}\Delta\Phi_{s,1} &= \Delta\mathrm{SWE}\cdot\frac{4\cdot\pi}{\lambda\cdot\rho_s}\cdot\left(\sqrt{\varepsilon_s(\rho_s)-\sin^2\theta_1}-\cos\theta_1\right)\\ &= \Delta\mathrm{SWE}\cdot\frac{4\cdot\pi}{\lambda\cdot\rho_s}\cdot\beta_1,\end{aligned} \tag{4}$$

$$\begin{aligned}\Delta\Phi_{s,2} &= \Delta\mathrm{SWE}\cdot\frac{4\cdot\pi}{\lambda\cdot\rho_s}\cdot\left(\sqrt{\varepsilon_s(\rho_s)-\sin^2\theta_2}-\cos\theta_2\right)\\ &= \Delta\mathrm{SWE}\cdot\frac{4\cdot\pi}{\lambda\cdot\rho_s}\cdot\beta_2,\end{aligned} \tag{5}$$

where θ_1 and θ_2 are the local incident angles of acquisitions S1 and S2, respectively and β_1 and β_2 are used as short hand notations from here on for the terms in the brackets. Following, the difference phase is

$$\Delta\Delta\Phi_s = \Delta\mathrm{SWE}\cdot\frac{4\cdot\pi}{\lambda\cdot\rho_s}\cdot(\beta_2-\beta_1) \tag{6}$$

and the ΔSWE can be estimated as

$$\Delta\mathrm{SWE} = \frac{\lambda\cdot\rho_s}{4\cdot\pi}\cdot\frac{\Delta\Delta\Phi_s}{\beta_2-\beta_1}. \tag{7}$$

Note that the accuracy of this approach is rather low since it is scaled by $\frac{1}{\beta_2-\beta_1}$ compared to the measurement using the single interferogram.

3.2 Absolute Phase and ΔSWE Estimation

In moderate- to high-coherence scenarios one can assume that a robust phase unwrapping is feasible. Still, the unwrapped interferograms may have an unknown bulk phase offset that needs to be resolved if no reference point is present in the scene. The bulk phase offset is an integer multiple of 2π. Similar to delta-k approaches for absolute phase estimation [9], the phase offset can be estimated from the difference phase. From (6) it follows that noisy versions of the absolute phase from acquisition S1 and S2 can be obtained as

$$\begin{aligned}\Delta\tilde{\Phi}_{s,1} &= \Delta\Delta\Phi_s\cdot\frac{\beta_1}{\beta_2-\beta_1}\\ \Delta\tilde{\Phi}_{s,2} &= \Delta\Delta\Phi_s\cdot\frac{\beta_2}{\beta_2-\beta_1},\end{aligned} \tag{8}$$

where the factor $\frac{\beta_i}{\beta_2-\beta_1}$ amplifies the phase noise on the difference phase. We can use the unwrapped phase $\Delta\Phi_{s,i,uw}$, which is equal to $\Delta\Phi_{s,i}$ except for the bulk phase offset, to estimate the integer multiple of the 2π phase offset according to

$$n_i = \left(\Delta\Delta\Phi_s\cdot\frac{\beta_i}{\beta_2-\beta_1}-\Delta\Phi_{s,i,uw}\right)\cdot\frac{1}{2\cdot\pi}, \tag{9}$$

where the index i indicates the respective acquisition, S1 or S2. This integer estimate can be averaged over the whole scene, i.e., over scene blocks in which a high confidence level in the phase unwrapping is ensured, to mitigate the high phase noise. An estimate of the single absolute phases with an accuracy and resolution like the interferograms is obtained as

$$\Delta\Phi_{s,i} = \Delta\Phi_{s,i,uw} + 2\cdot\pi\cdot n_i. \tag{10}$$

3.3 Permittivity and Density Estimation

In contrast to delta-k approaches, the phase ratio of the interferograms can be used to estimate the permittivity, hence, the density of the accumulated snow. The ratio can be written as

$$\frac{\Delta\Phi_{s,1}}{\Delta\Phi_{s,2}} = \alpha = \frac{\sqrt{\varepsilon_s-\sin^2\theta_1}-\cos\theta_1}{\sqrt{\varepsilon_s-\sin^2\theta_2}-\cos\theta_2}, \tag{11}$$

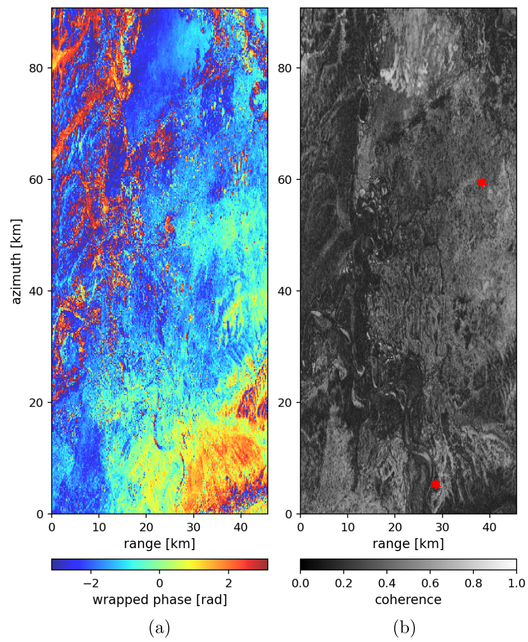

Figure 6 Products from the InSAR processing of the Sentinel-1 D-InSAR pair showing in radar coordinates: (a) the topography corrected wrapped phase and (b) the interferometric coherence. Red stars indicate the location of the snow measurement sites.

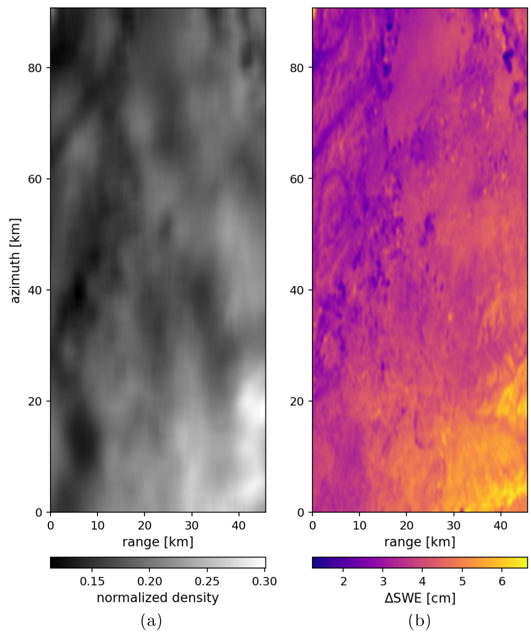

Figure 7 (a) semi-physically simulated density map and (b) ΔSWE map resulting from the inversion of the interferometric phase, the density map, and the local incident angles. Both used as input to the simulation.

where α is used from here on as a short hand notation for the phase ratio. Solving (11) for the permittivity results in two roots. One root is equal to 1 and the other, the physical one, can be written as

$$\varepsilon_s = \frac{1}{(\alpha^2-1)^2} \cdot \left[-4 \cdot \alpha \cdot \cos\theta_1 \cdot \cos\theta_2 \cdot \left(\alpha^2+1\right) + 2 \cdot \alpha^2 \cdot (\cos 2\theta_1 + \cos 2\theta_2) + \alpha^4 + 2 \cdot \alpha^2 + 1\right]. \quad (12)$$

Note that α is independent of the snow height, i.e., the SWE. Hence, only information on the acquisition geometry is required for estimating the permittivity. Using the relation in (3), the density can be estimated from ε_s.

4 Simulation Results

To test the validity of the proposed approaches, we use simulated Sentinel-1/Harmony acquisitions on a single look complex (SLC) level, derived from a real Sentinel-1 D-InSAR acquisition over Alaska for which prove of a significant snowfall event is provided by a snow depth measurement station within the extent of the scene.

Two Sentinel-1 IW images, acquired at January 28, 2020 and February 9, 2020, are used to form the D-InSAR acquisition. The scene is located in western Alaska with the scene center at at $64°41'48''$ N and $156°42'54''$ W. **Figure 6** shows the wrapped D-InSAR phase (surface topography removed using the 30 m TanDEM-X DEM) and the coherence. Only one sub-swath is used. The formulation in (2) is used to retrieve the ΔSWE map from the unwrapped interferogram. Since no information on the snow density is available we assume a synthetically generated density distribution shown in panel (a) of **Figure 7**. The resulting ΔSWE map is shown in panel (b). Note that we used the data from two snow measurement stations within the scene to calibrate (i.e., offset) the ΔSWE map. The location of the sites is indicated by red stars in Figure 6.

To generate the SLCs, for both the Sentinel-1 and Harmony acquisitions, we use the amplitude images of the real Sentinel-1 scene as reflectivity map, multiplied by independent realizations of high-resolution speckle. The coherence and phase are injected in form of a complex coherence in both of the D-InSAR pairs by means of a 2-image Cholesky decomposition. The amplitude of the complex coherence is assumed to be equivalent for both interferograms and corresponds to the real Sentinel-1 coherence map (cf. panel (b) in Figure 6). The phase of the coherence represents the ΔSWE phase and is computed according to (2) assuming the derived ΔSWE and density maps shown in Figure 7 and the respective local incident angle maps for the Sentinel-1 and Harmony acquisition. For the Sentinel-1 acquisition, the local incident angles correspond to the real acquisition. The Harmony satellite is assumed to be flying on the same orbit but 350 km behind the Sentinel-1 satellite, receiving the scattered echoes from Sentinel-1 in a receive only configuration, as foreseen for the Harmony constellation [6]. The incident angles are mapped accordingly to this squinted acquisition. The bistatic nature of the Harmony acquisition is considered in the simulation.

4.1 Low-Resolution ΔSWE Estimation

We use the procedure described in Subsection 3.1 to obtain a low-resolution estimate of the ΔSWE distribution. Note that no phase unwrapping is required. We assume at this point that the density (i.e., permittivity) distribution is

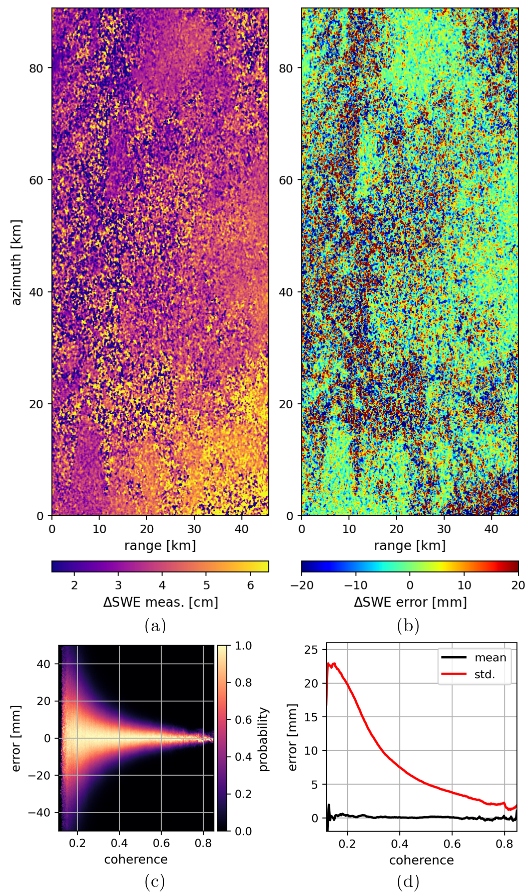

Figure 8 Results of the low-resolution ΔSWE inversion, showing (a) the retrieved ΔSWE map, (b) the estimation error, and (c) and (d) the error statistics in form of a 2-D histogram as well as mean and standard deviation values for different coherence values.

known. The density inversion is outlined in the following section. **Figure 8** shows the result of the inversion according to formula (7). The retrieved ΔSWE map is shown in panel (a). A multi-look (ML) window of 400 m x 400 m was used. The retrieved ΔSWE distribution resembles the one used as an input to the simulation (cf. panel (b) of Figure 7) but is very noisy in low-coherence areas. The error of the ΔSWE measurement is shown in panel (b) and error statistics are given in panels (c) and (d) in form of a 2-D histogram and mean and standard deviation values of the error for different coherence levels over the scene. Note that the histogram is normalized for each coherence bin. Note also that pixels with coherence values < 0.1 were masked for the inversion. The statistics in panel (d) show that the inversion is unbiased and for the used ML window, sub-centimeter accuracy is reached for coherence values > 0.4. The accuracy may be increased by using larger windows, on the cost of a reduced spatial resolution.

4.2 Absolute Phase, ΔSWE, and Density Estimation

Here, we are presenting a joint inversion of the ΔSWE and the density by means of the absolute phase estimation and permittivity estimation strategies outlined in Subsections 3.2 and 3.3, respectively. As an initial guess, a constant normalized density of $\rho_s = 0.1$ is assumed over the scene. A single bulk phase offset is computed for the whole scene, since a consistent unwrapping was possible over the whole extent of the scene. The estimated bulk phase offset results in $1 \cdot 2\pi$ for both the Sentinel-1 and Harmony interferogram. The absolute phase is obtained as the unwrapped phase plus the bulk offset. Panel (a) of **Figure 9** shows the ΔSWE retrieved from the estimated absolute phase. The distribution is well resolved and resembles the original one in Figure 7. The estimation error is shown in panel (b), where a systematically varying bias is present, caused by the inaccurate initial density estimate. We use the approach from Section 3.3 to estimate the permittivity from the absolute phase and the formulation in (3) to retrieve the density. A large ML window of 500 m x 500 m is used in the permittivity estimation to mitigate the strong noise on the ratio of the interferograms that is used for the inversion. The ΔSWE inversion is then performed again with the estimated permittivity and density. Panel (d) of Figure 9 shows the error of the finally retrieved ΔSWE. Note that we performed the ΔSWE inversion from the estimated absolute phases of both the Sentinel-1 and Harmony interferogram and averaged the resulting products to further improve the accuracy. The error statistics for the density estimate and the final ΔSWE estimate are shown in panels (e)-(h) for different coherence values. We result in an accuracy around 1 mm for the present example using a ML window of 50 m x 50 m.

5 Concluding Remarks

In this paper, the potential of multiple simultaneous D-InSAR acquisitions with different squints for the estimation of snow parameters has been demonstrated. The phase difference between the interferograms can be exploited to directly obtain an unbiased ΔSWE estimate without the need for phase unwrapping and without a reference point within the scene. Furthermore, the ratio of the two interferograms is a measure of the dielectric permittivity of the snow and hence, can be inverted to the density of the snow. ESA's Harmony mission or the Co-Flier concepts from NASA JPL, may be the perfect candidates to implement these techniques. Systematic biases and a deterioration of the accuracy may arise from atmospheric effects, coregistration errors between the two acquisition geometries, as well as orbit, baseline and attitude knowledge errors. These error sources have not been treated in the scope of this paper. A detailed study of the potential error sources is left for future research.

6 Acknowledgment

Andreas Benedikter would like to thank Prof. Helmut Rott (ENVEO) for the valuable discussions.

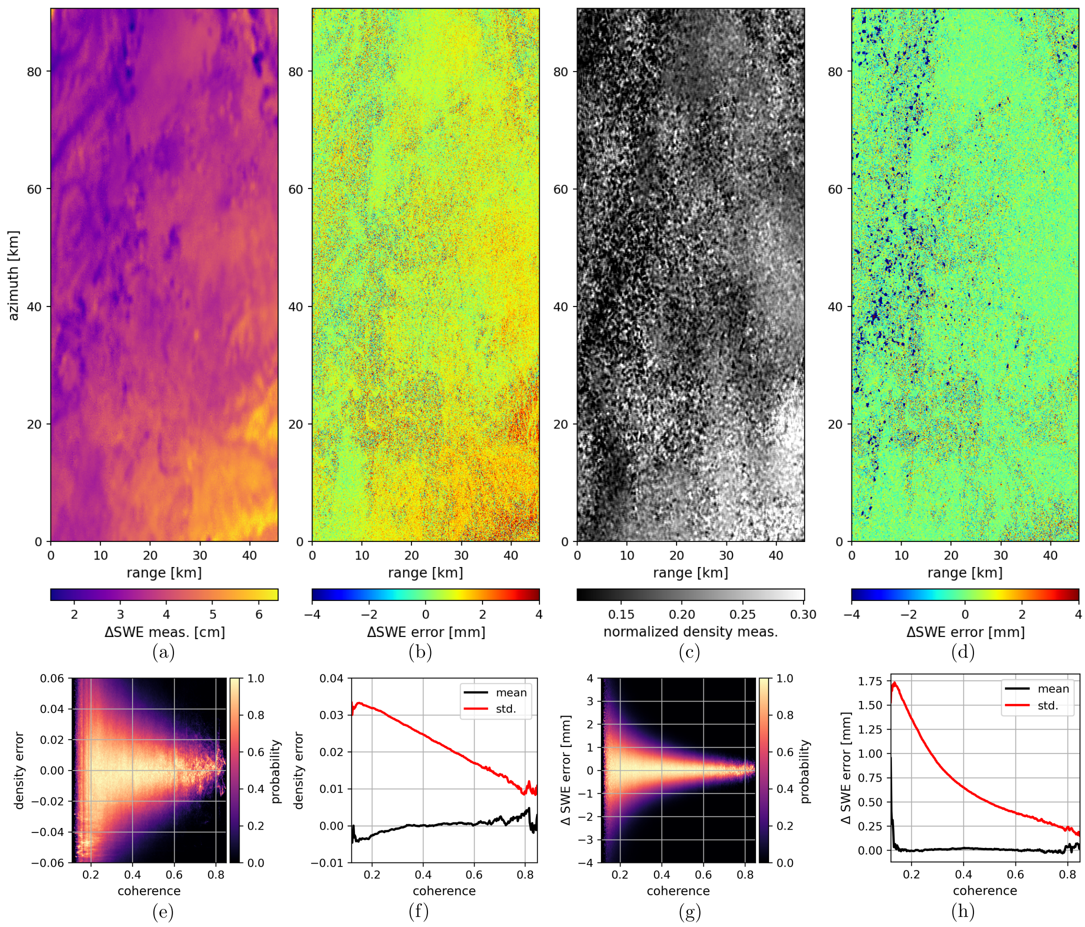

Figure 9 Results from the absolute phase and density estimation, showing (a) the retrieved ΔSWE from the absolute phase using an initial density estimate of 0.1, (b) the ΔSWE measurement error that shows systematic biases resulting from the inaccurate initial density estimate, (c) measured density, (d) resulting ΔSWE error when using the measured density in the inversion, (e) and (f) error statistics of the density estimate, and (g) and (h) error statistics of the final ΔSWE estimate.

7 Literature

[1] T. Guneriussen *et al.*, "InSAR for estimation of changes in snow water equivalent of dry snow," *IEEE Transactions on Geoscience and Remote Sensing*, vol. 39, no. 10, pp. 2101–2108, 2001.

[2] H. Rott, T. Nagler, and R. Scheiber, "Snow mass retrieval by means of SAR interferometry," in *3rd Fringe Workshop Eur. Space Agency Earth Observ.*, 2004.

[3] S. Leinss, A. Wiesmann, J. Lemmetyinen, and I. Hajnsek, "Snow water equivalent of dry snow measured by differential interferometry," *IEEE Journal of Selected Topics in Applied Earth Observations and Remote Sensing*, vol. 8, no. 8, pp. 3773–3790, 2015.

[4] K. Belinska, G. Fischer, T. Nagler, and I. Hajnsek, "Snow water equivalent estimation using differential SAR interferometry and co-polar phase differences from airborne SAR data," in *IGARSS 2022 - 2022 IEEE International Geoscience and Remote Sensing Symposium*, pp. 4545–4548, 2022.

[5] Y. Li *et al.*, "Differential tropospheric delay estimation by simultaneous multi-angle repeat-pass InSAR," *IEEE Transactions on Geoscience and Remote Sensing*, vol. 60, pp. 1–18, 2022.

[6] ESA (2022), "Earth Explorer 10 candidate mission Harmony," tech. rep., European Space Agency, Noordwijk, The Netherlands, ESA-EOPSM-HARM-RP-4129, 369pp.

[7] M. Lavalle *et al.*, "Co-fliers concepts formulation for NISAR and ROSE-L to address SDC and STV needs," in *IGARSS 2023 - 2023 IEEE International Geoscience and Remote Sensing Symposium*, 2023.

[8] P. López-Dekker *et al.*, "The Harmony mission: End of Phase-0 science overview," in *2021 IEEE International Geoscience and Remote Sensing Symposium IGARSS*, pp. 7752–7755, 2021.

[9] S. Madsen, H. Zebker, and J. Martin, "Topographic mapping using radar interferometry: processing techniques," *IEEE Transactions on Geoscience and Remote Sensing*, vol. 31, no. 1, pp. 246–256, 1993.